Harnessing Photochemical Shrinkage in Direct Laser Writing for Shape Morphing of Polymer Sheets

Anton Bauhofer, Sebastian Krödel, Jan Rys, Osama R. Bilal, Andrei Constantinescu, Chiara Daraio

Harnessing Photochemical Shrinkage in Direct Laser Writing for Shape Morphing of Polymer Sheets

Anton A. Bauhofer, Sebastian Krödel, Jan Rys, Osama R. Bilal, Andrei Constantinescu, and Chiara Daraio

Structures that change their shape in response to external stimuli unfold possibilities for more efficient and versatile production of 3D objects. Direct laser writing (DLW) is a technique based on two-photon polymerization that allows the fabrication of microstructures with complex 3D geometries. Here, it is shown that polymerization shrinkage in DLW can be utilized to create structures with locally controllable residual stresses that enable programmable, self-bending behavior. To demonstrate this concept, planar and 3D-structured sheets are preprogrammed to evolve into bio-inspired shapes (lotus flowers and shark skins). The fundamental mechanisms that control the self-bending behavior are identified and tested with microscale experiments. Based on the findings, an analytical model is introduced to quantitatively predict bending curvatures of the fabricated sheets. The proposed method enables simple fabrication of objects with complex geometries and precisely controllable shape morphing potential, while drastically reducing the required fabrication times for producing 3D, hierarchical microstructures over large areas in the order of square centimeters.

Programming shapes in planar materials enables the transformation of 2D sheets into controllable, 3D geometries.[1,2] This programmability expands the potential of available micro- and nanofabrication techniques and increases the fabrication throughput for objects with complex geometries[3] or origami structures.[4] Various physical effects have been exploited to produce structures that can change shape in a controlled manner, allowing for efficient fabrication of versatile geometries.[1] Among others, residual-stress-driven approaches have been explored to acquire self-bending behavior through gradients in thermal expansion,[5] anisotropic swelling,[6] differential lattice constants,[7,8] or buckling of prestrained substrates.[9,10] Recently, residual stresses induced by polymerization were also used to produce structures with shape morphing potential.[11,12] Applications of programmable materials have been suggested in microrobotics,[13,14] biomedical devices,[15,16] and biomimetic systems.[6,17] However, most of the reported approaches require complex fabrication processes, including composites or multiple materials, or are limited to specific geometries or the use of soft materials.[18] Besides, most realizations of programmable materials have to date been demonstrated for macroscopic structures, in the centimeter and millimeter scales.

Here, we show a method to create microscale, programmable geometries by inducing residual stresses during direct laser writing (DLW) of photocurable polymers. DLW is a commonly used technique for the fabrication of microscale 3D structures. The technique is based on two-photon polymerization of photosensitive, liquid oligomers, generated by local exposure to a pulsed laser beam.[19–21] A byproduct of DLW is the presence of residual stresses, caused by incompatible strains due to nonuniform laser exposure, which result in undesirable shrinkage and distortions of the fabricated samples. The occurring deformations have been characterized in prior studies[22] and corrected through chemical alternations of photoresists[23] and geometrical precompensation of the expected deformations.[24] Here, we exploit these residual stresses to program thin, 2D sheets that reconfigure into 3D shapes. The reconfiguration is triggered by capillary forces, acting on the sheets during the drying process, after the fabrication steps of polymerization and developing.[25,26] The bending directions and angles in the resulting deformations are controlled by locally varying geometrical and writing parameters, opening a broad space for design. This approach allows for direct programmability of 3D-structured single-material sheets in a simple fabrication process, thus minimizing time and complexity in manufacturing.

The fabrication process and the bending mechanism are summarized in **Figure 1**. During DLW, a femtosecond laser is redirected and focused inside a droplet of photoresist, to induce local polymerization (Figure 1a). Due to the high laser intensity in the focal point, photoinitiator molecules in the photoresist are radicalized and trigger a chain reaction of the surrounding oligomers. In this process, oligomers are transformed into a dense polymer-network via photoinduced crosslinking

A. A. Bauhofer, S. Krödel, J. Rys, Dr. O. R. Bilal
Department of Mechanical and Process Engineering
Swiss Federal Institute of Technology (ETH)
8092 Zurich, Switzerland
A. A. Bauhofer, S. Krödel, J. Rys, Dr. O. R. Bilal, Prof. C. Daraio
Department of Mechanical and Civil Engineering
California Institute of Technology
Pasadena, CA 91125, USA
E-mail: daraio@caltech.edu
Prof. A. Constantinescu
Laboratoire de Mécanique des Solides
CNRS UMR7649
Ecole Polytechnique
91129 Palaiseau Cedex, France

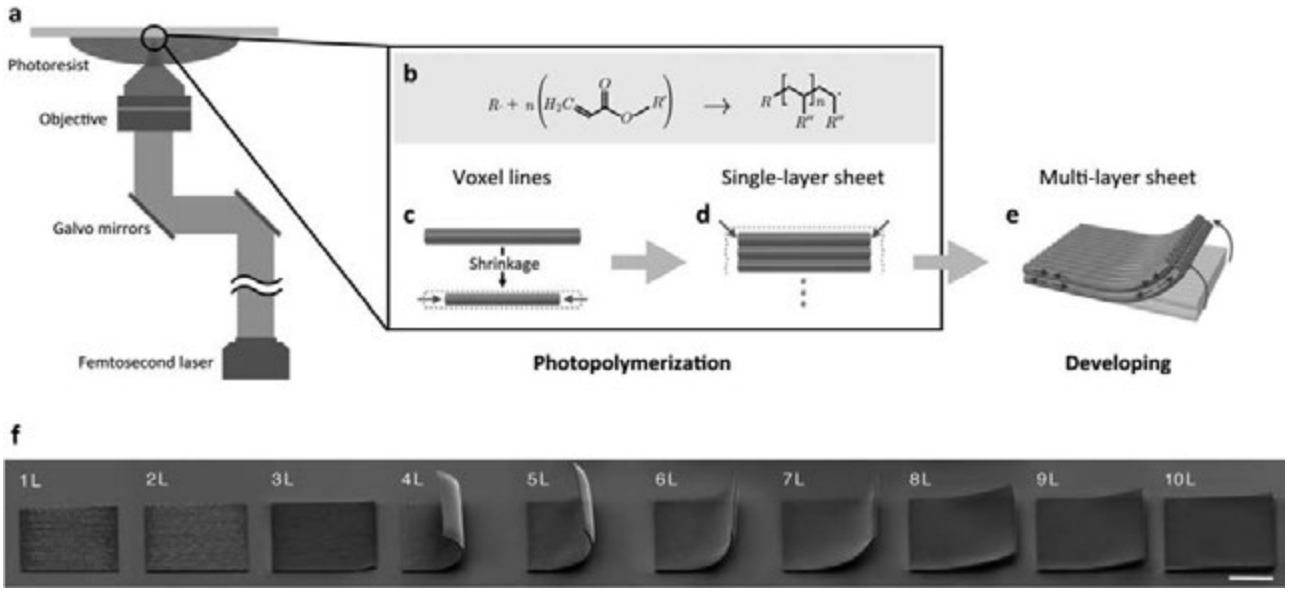

Figure 1. Direct laser writing (DLW) of prestrained sheets prone to self-bending. a) An 80 MHz femtosecond laser is redirected and focused with galvo mirrors and an objective into a droplet of photoresist to cause local photopolymerization in the focal point. b) Representative radical polymerization reaction of oligomers with acrylate end-groups. c) The chemical reactions at the molecular level induce a macroscopic volumetric shrinkage, denoted as polymerization shrinkage. d) Layers of polymerized material are created by laser writing of parallel voxel lines. Crosslinking of adjacent voxel lines causes shrinkage in all lateral directions. e) Successive shrinkage of stacked layers induces a bending moment that enables out-of-plane deflections. f) SEM images of different self-bent sheets containing 1 to 10 (from left to right) stacked layers of parallel voxel lines that were successively written from bottom to top. Scale bar: 100 μm.

(Figure 1b). The formation of covalent bonding between the oligomers locally reduces the average atomic distance in the resist,[27] leading to an increased density at the molecular level. At the macroscopic level, this induces shrinkage and distortions of the polymerized volumes (Figure 1c). By scanning the laser focal point along a prescribed trajectory, regions that experience shrinkage can be formed with almost arbitrarily complex geometries. These regions can then be utilized to evoke shape-changing behavior. Laser writing a sheet of parallel adjacent voxel lines leads to crosslinking of the polymerized regions, causing collective in-plane shrinkage (Figure 1d). During consecutive writing of multiple stacked layers, interconnectivity of the layers inhibits further in-plane shrinkage and results in the emergence of residual stresses that create an out-of-plane bending moment (Figure 1e). After laser writing, a developing process dissolves and washes off the remaining resist. During drying, the surface tension of the washing liquid outweighs adhesive forces between the structures and the underlying substrates, triggering delamination of the sheets from the substrates and out-of-plane bending. We fabricated and analyzed sheets of stacked layers with a thickness of $t = 0.5$ μm and lateral dimensions of 250 μm × 250 μm (Figure 1f). The resulting bending curvatures of the sheets are strongly dependent on the laser writing trajectories and the number of stacked layers, which dictate the magnitude of the residual stresses as well as the bending rigidity of the sheets. Stress concentrations within the sheets cause delamination to begin from the sheet edges and then propagate inward (see Supporting Information).

To understand the fundamental mechanisms of self-bending induced by photopolymerization, we designed controlled experiments to identify the driving physical effects. We determined that i) capillary action, ii) residual stresses, and iii) adhesive forces are the main influence factors controlling the resulting bending curvatures and geometries (**Figure 2**a). First, we investigated the influence of capillary action on the bending, which occurs after developing of the polymer, by applying different drying procedures and rinsing liquids to separate samples. To test the influence of different surface energies of the rinsing liquid, we immersed developed samples in water and isopropanol (IPA) and measured the receding contact angle of the liquids on the sheets (Figure 2b). When the samples were dried in water, we observed evaporation with a pinned contact line at the sheet edges and a receding contact angle of $\theta_{R,water} = 40.5° \pm 0.1°$. Due to the high surface energy of the liquid, the tested samples were completely detached from the substrates. During drying of samples in IPA, we observed no pinned contact line, due to the low surface energy of IPA, and a constant contact angle of $\theta_{R,IPA} = 16° \pm 1°$. By using IPA as drying liquid, we achieved controlled repeatable detachment and self-bending. We also performed control experiments using critical point drying (CPD), where no capillary actions occur. In this case, the samples did not show any significant bending, demonstrating the relevant role played by capillary action on the programmability of the final shapes.

Next, we analyzed the residual stresses that form during photopolymerization. For the chosen DLW parameters (see Experimental Section), we identified voxel lines with ellipsoidal cross-sections with a width and height of 0.37 ± 0.03 μm and 2.07 ± 0.20 μm and a longitudinal strain of $\varepsilon_l = 16.3 \pm 1.1\%$ that occurs during solidification of the photoresist (see Supporting Information). Crosslinking between consecutively written voxel lines restrains shortening of the lines, resulting in a reduced

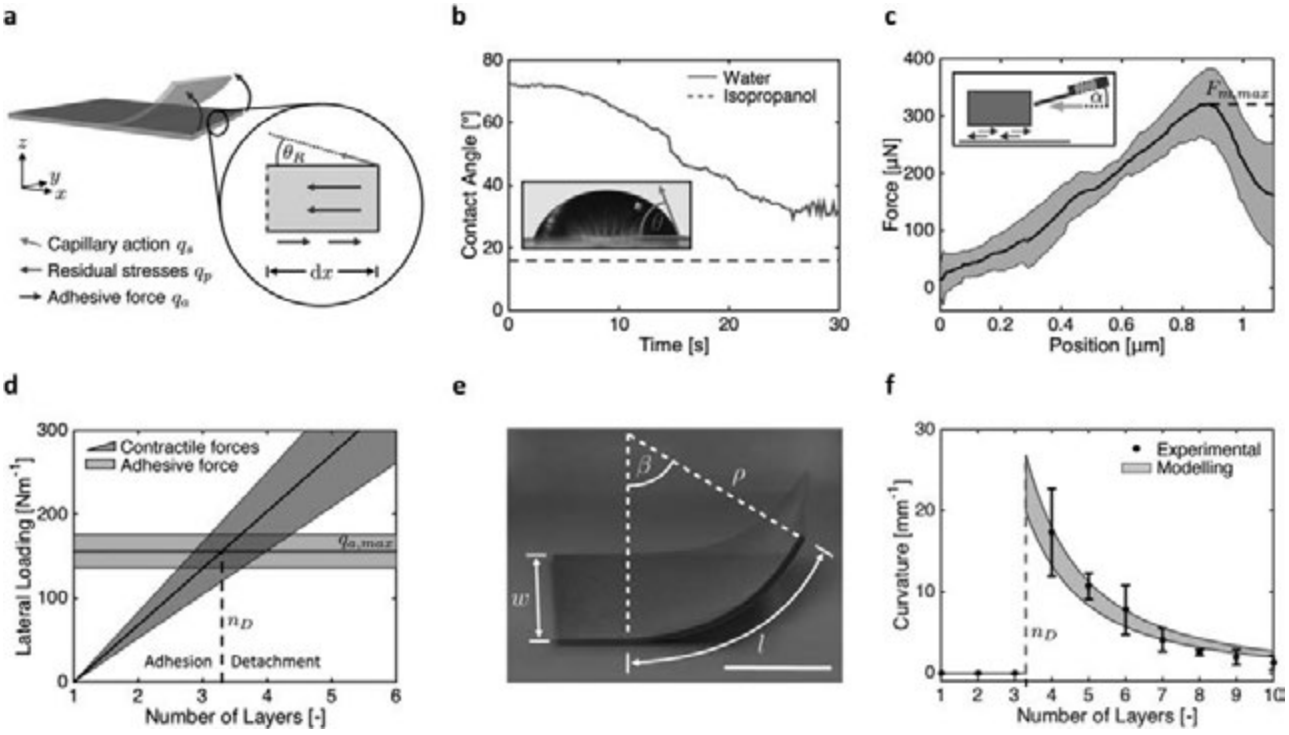

Figure 2. Self-bending mechanism of laser-written sheets, detaching from the substrate. The shaded areas in panels c–f indicate the standard deviations computed from the measurement results with Gaussian error propagation. a) Schematic diagram showing the lateral forces acting along the border of detachment on a line element with infinitesimal width d*x*. b) Measured receding contact angles of water and IPA on a substrate produced by DLW. The inset shows the contact angle of a water droplet. c) Measurements of the lateral adhesive forces between the photopolymer and the glass substrate. The inset depicts the experimental setup. d) The experimentally determined contractile line loads from the capillary action and the residual stresses are compared to the maximum adhesive line force $q_{a,max} = \tau_{max} \times w$. Delamination is expected for sheets with a number of layers above the critical number $n_D = 3.30$, when the contractile forces overcome the maximum adhesion. e) Self-bent sheet with an angle of curvature β, a radius of curvature ρ, a width w, and an arc length l. Scale bar: 100 μm. f) Comparison of the analytical predictions with experimental data for the final bending curvature obtained with samples composed of different numbers of layers. The error bars indicate the standard deviation determined from measurements on 10 samples per data point.

in-plane macroscopic shrinkage within sheets. We used optical microscopy to observe photochemical shrinkage in-situ during DLW and evaluated the macroscopic shrinkage of sheets with scanning electron microscopy (SEM). For ten evaluated, unrestricted single-layer sheets with parallel voxel lines, a mean polymerization shrinkage-induced strain of $\varepsilon_p = 3.7 \pm 0.5\%$ was found. This value agrees with prior literature.[28] The consequent residual stresses that occur during DLW are calculated as $\sigma_r = (1 - \nu)^{-1} \times \varepsilon_p \times E$, where E and ν denote the Young's modulus and the Poisson's ratio of the polymerized material. To characterize the mechanical properties of the polymer sheets, we applied nanoindentation (see Supporting Information). We obtained a Young's Modulus of $E = 1.86 \pm 0.15$ GPa in accordance with prior literature,[29] while assuming a Poisson's ratio of $\upsilon = 0.49$.[29]

For measuring the lateral adhesive forces between the polymer sheets and adjacent glass substrates, we used a micromechanical testing system (see Experimental Section). We pushed a laser written cube on the glass surface and measured the resulting force with a capacitive force sensor (Figure 2c). A maximum lateral adhesion tension of $\tau_{max} = \frac{F_{m,max}}{\cos\alpha \times A_m} = 623.9 \pm 80.7$ kPa was determined, where $F_{m,max} = 321.7 \pm 61.9$ μN denotes the maximum measured force, $\alpha = 15°$ the mounting angle of the sensor, and $A_m = 625$ μN^2 the surface area of the test cube.

We develop a mechanical model to inform the experimental observations and quantitatively predict delamination and self-bending angle of multilayered sheets for design. In the model, we account for the fact that detachment and bending angle are both highly sensitive to the number of stacked layers n (Figure 1f). From experimental observations, we consider two distinct regimes: i) sheets with a low number of layers ($n \leq n_D$) that undergo no delamination, and ii) sheets with a high number of layers ($n > n_D$) that experience delamination and subsequent self-bending into specific curvatures. n_D is thereby introduced as a critical number to locate the point of delamination.

To determine the critical number n_D, we derive a delamination condition that balances the in-plane forces acting in tangent direction at the delaminating edge (Figure 2a). Line loads in an element with infinitesimal width dx are calculated to capture the experimentally measured effects. The line load imposed by capillary action during drying is computed as $q_s = \cos\theta_R \times \gamma_{lv}$, where we assume the surface tension between the liquid and the vapor phase of IPA to be $\gamma_{lv,\,IPA} = 21.0 \times 10^{-3}$ N m^{-1}. The impact of residual stresses is computed by integration of the residual stresses over the total sheet height $q_r = \int_t^{n \times t} \sigma_r \, dz$, where the

thickness of the stacked layers is denoted as t. We assume a uniform stress distribution in the cross-sections of the stacked layers ($\varepsilon_i = \varepsilon_p$, $i > 1$), while the first layer ($i = 1$) is presumed to experience unconstrained shrinkage. The total compressive line force at the delaminating edge amounts to the sum of the line loads due to the two effects $q_c = q_s + q_r$. The maximum adhesion between the line element and the substrate is calculated as $q_{a,max} = \tau_{max} \times w$, where w denotes the lateral sheet dimension. Delamination is predicted if the contractile forces outweigh the adhesion of the line element $q_c > q_a$. Based on the experimental results, the critical number is computed as $n_D = 3.30 \pm 0.86$ (Figure 2d).

The self-bending curvatures of the sheets after delamination are predicted with a simplified model based on multilayer beam bending theory. Sheets in a cylindrical bending configuration are considered in a state of minimal stresses. Curvatures normal to the cylindrical bending are assumed to be zero, thus reducing the model to a 1D system that can be approximated with beam theory. All stresses in an element of the bent beam portion are represented by n, tensile forces P_i, and bending moments M_i for the distinct layers (see Supporting Information).[30,31] In the final sheet configuration, no external forces or moments act on the bent region of the sheets, leading to force and moment equilibria that only contain the introduced loads P_i and M_i. The constitutive equations for the layers are $M_i = \frac{E_i I_i}{\rho}$, where E_i and I_i represent the Young's Moduli and the moments of inertia, while ρ is referred to as the radius of curvature and is defined as the reciprocal value of the curvature $\rho = \frac{1}{\kappa}$. In addition, we introduce a compatibility condition for the strains in adjacent layers

$$\varepsilon_{p,i} - \varepsilon_{p,i+1} = \frac{P_i}{w t_i E_i} - \frac{P_{i+1}}{w t_{i+1} E_{i+1}} - \frac{t_i + t_{i+1}}{2\rho} \tag{1}$$

We assume that cross-sections which are plane and perpendicular to the neutral axis remain in that condition and that out-of-plane tensions related to edge effects are negligible. Furthermore, the sheet thickness is assumed to be much smaller than the lateral sheet dimensions $\left(\sum_n t_i \ll w\right)$, while the distinct layers are approximated to be homogeneous and isotropic. The resulting closed-form solution (see Supporting Information) is

$$\kappa = \frac{6 \sum_{i=1}^{n} \sum_{j>i}^{n} t_i t_j \left(\varepsilon_i - \varepsilon_j\right)}{\left(\sum_{i=1}^{n} t_i\right)^3} \tag{2}$$

To achieve controlled adhesion, the first written layer is partly immersed in the substrate. Therefore, we assume half of the thickness for the first layer $\left(t_1 = \frac{1}{2} t\right)$ (see Supporting Information). For all proceeding layers, the thickness is assumed to be constant ($t_i = t$, $i > 1$). With these assumptions and the introduced delamination condition, the solution expressed in Equation (2) can be simplified to

$$\kappa = \begin{cases} 0, & n \le n_D \\ \frac{24\varepsilon_p}{t} \times \frac{n-1}{8n^3 - 12n^2 + 6n - 1}, & n > n_D \end{cases} \tag{3}$$

We compare the predicted curvatures from the model to the experimentally determined curvatures of laser written sheets (Figure 2f). The model and the experimental results agree for both the nondelaminated and the self-bent regions. We determined the bending angles β of the bent sheets with SEM imaging, by measuring the tangential slopes of the free edges (Figure 2e). The viewing angle δ was corrected with $\beta = \frac{\beta'}{\cos\delta}$, where β' denotes the projected bending angle in the SEM image. We computed the curvatures from the bending angles as $\kappa = \frac{\beta}{l}$, where the arc length is denoted as l.

The presented experimental approach, paired with our predictive analytical tool, enables the direct fabrication of microscale shape morphing structures with designed bending curvatures and shapes. This method can be used to produce 3D structures at a fraction of the time and fabrication costs compared to their realization by DLW (without shape morphing). To demonstrate the potential of our approach, we fabricated self-bending sheets that evolved into lotus-like microcontainers upon drying (**Figure 3**a). We controlled the bending curvatures by varying the number of stacked layers. Positive Gaussian curvatures were achieved by stacking of layers with differently oriented voxel lines. While the microcontainers could also be fabricated by conventional DLW, laser writing time was reduced by a factor of ≈4 when fabricated using self-bending sheets (the sheets required a writing time of $T_S = 5.5 \pm 0.5$ s, whereas the direct writing of the final, spherical geometry took $T_o = 19.0 \pm 0.5$ s, see Supporting Information). A potential application for the self-bending geometry can be found in drug delivery, where the approach could be applied to biodegradable materials that exhibit photochemical shrinkage.[16,32,33]

Our method can also be used to create programmable anisotropic and inhomogeneous surfaces that replicate functionalities found in nature (Figure 3b). For example, shark skin topology is known to enhance swimming speed and agility of the fish, by creating a leading-edge vortex.[34] We fabricated a biomimetic shark skin in the form of a 3D-structured sheet with structured microfins. To locally control bending, we increased the sheet thickness in selected locations (see inset of Figure 3c). These variations in thickness enable localized self-bending and lead to the formation of structures that mimic the geometry and feature sizes of natural shark skins. Using DLW, surfaces in the cm-range can be produced in a single production cycle (see Supporting Information).

In conclusion, we show that DLW can be used to create microstructures with programmable self-bending behavior. All driving physical effects for the acquired shape transformations have been identified and evaluated using ad-hoc microscale experiments. We present a mechanical model that predicts bending curvatures based on the measured parameters. Due to the flexibility of the fabrication process, our approach opens prospects for a fast and simple creation of shape morphing structures with complex geometries.

Experimental Section

Photolithography: The self-bending microstructures were fabricated with the commercial DLW system Photonic Professional GT by Nanoscribe GmbH. The photoresist IP-Dip (Nanoscribe GmbH,

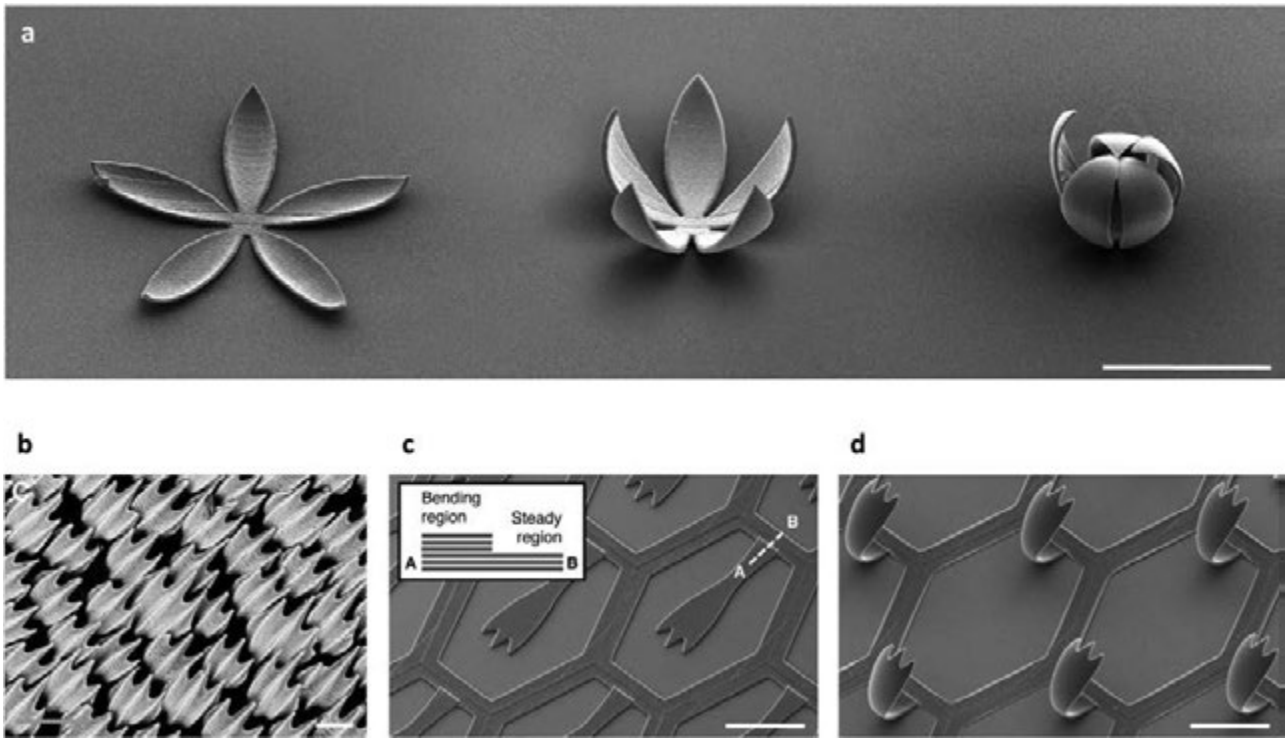

Figure 3. SEM images of biomimetic sheets with controlled self-bending capability. Scale bars: 100 µm. a) Lotus flower geometries with varying numbers of layers and different resulting bending curvatures. b) Microscopy image of a natural shark skin. Reproduced with permission.[34] Copyright 2014, The Company of Biologists Ltd. c) Micropatterned surface prior to self-bending. The inset depicts the thickness profile of the sheet that was implemented to achieve local control of the bending. d) Micropatterned surface after self-bending. The surface was designed to replicate the drag-reducing effect of a natural shark skin.

Eggenstein-Leopoldshafen, Germany) and a 25× objective with a numerical aperture of 0.8 and a working distance of 390 µm were used in galvo scan mode in dip-in laser lithography configuration. Laser power (LP = 16 mW), scan speed (SS = 55 000 µm s^{-1}), and galvo settling time (GT = 2 ms) were kept constant during writing, while slicing and hatching distances were set to 0.5 and 0.3 µm. The implemented parameters and materials serve as a benchmark whereby qualitatively equivalent results would be expected for the use of other resists. The observed effects could be potentially maximized with resists that feature stronger polymerization shrinkage.[35] Multilayered sheets of parallel voxel lines were made with the dimensions 250 µm × 250 µm × (n − 0.5) × 0.5 µm with n being the number of stacked layers. The laser written structures were developed with the solvent mr-Dev 600 (Micro Resist Technologies GmbH, Berlin, Germany) for 12 min, rinsed in IPA for 3 min, and air-dried in horizontal orientation in steady air. The receding contact angle of IPA on the samples during evaporation was measured with a DSA100 drop shape analyzer (Krüss Ltd., Hamburg, Germany). To verify that capillary forces act as trigger for the self-bending behavior of the laser written sheets, CPD, during which no capillary actions occur, was performed in comparison to air drying. No self-bending curvatures were observed in sheets that were subjected to CPD.

Micromechanical Testing: We applied a micromechanical compressions sense system (FemtoTools AG, Zurich, Switzerland) for measuring the adhesive forces between laser written structures and uncoated glass substrates. A FT-L1000 sensing probe with a force range of ± 1000 µN and a resolution of 0.05 µN was used with a 50 µm × 50 µm tip to measure the occurring forces during lateral movement of blocks of polymerized photoresist with the dimensions 25 µm × 25 µm × 25 µm. The material properties of the constituent polymer film were measured using a nanoindenter (TriboIndenter, Hysitron Inc., USA) equipped with a 5 µm, 60° conical tip. All measurements were carried out in a displacement-controlled mode with an indentation depth of 2.0 µm. Each measurement consisted of a loading function including a loading (10 s) and an unloading (10 s) segment. The material properties of five individual samples were determined on four different positions around the center of the film. The reduced Young's modulus was determined by the Oliver and Pharr method.[36]

Acknowledgements

This work was partially funded by the Swiss National Science Foundation through grant "MechNanoTruss–Mechanical response of polymer nanotruss scaffolds" (No. 164375).

Conflict of Interest

The authors declare no conflict of interest.

Keywords

direct laser writing, residual stresses, self-bending, shape programming

[1] Y. Liu, J. Genzer, M. D. Dickey, *Prog. Polym. Sci.* **2016**, *52*, 79.
[2] R. Kempaiah, Z. Nie, *J. Mater. Chem. B* **2014**, *2*, 2357.
[3] Z. X. Khoo, J. E. M. Teoh, Y. Liu, C. K. Chua, S. Yang, J. An, K. F. Leong, W. Y. Yeong, *Virtual Phys. Prototyping* **2015**, *10*, 103.
[4] J. H. Na, A. A. Evans, J. Bae, M. C. Chiappelli, C. D. Santangelo, R. J. Lang, T. C. Hull, R. C. Hayward, *Adv. Mater.* **2015**, *27*, 79.
[5] J. Kim, J. A. Hanna, M. Byun, C. D. Santangelo, R. C. Hayward, *Science* **2012**, *335*, 1201.
[6] A. S. Gladman, E. A. Matsumoto, R. G. Nuzzo, L. Mahadevan, J. A. Lewis, *Nat. Mater.* **2016**, *15*, 413.
[7] O. G. Schmidt, K. Eberl, *Nature* **2001**, *410*, 168.
[8] A. Cho, *Science* **2006**, *313*, 164.
[9] Y. Sun, W. M. Choi, H. Jiang, Y. Y. Huang, J. A. Rogers, *Nat. Nanotechnol.* **2006**, *1*, 201.
[10] S. Xu, Z. Yan, K.-I. Jang, W. Huang, H. Fu, J. Kim, Z. Wei, M. Flavin, J. McCracken, R. Wang, A. Badea, Y. Liu, D. Xiao, G. Zhou, J. Lee, H. U. Chung, H. Cheng, W. Ren, A. Banks, X. Li, U. Paik, R. G. Nuzzo, Y. Huang, Y. Zhang, J. A. Rogers, *Science* **2015**, *347*, 154.
[11] Z. Ding, C. Yuan, X. Peng, T. Wang, H. J. Qi, M. L. Dunn, *Sci. Adv.* **2017**, *3*, e1602890.
[12] Z. Zhao, J. Wu, X. Mu, H. Chen, H. J. Qi, D. Fang, *Sci. Adv.* **2017**, *3*, e1602326.
[13] E. W. H. Jager, O. Inganäs, I. Lundström, *Science* **2000**, *288*, 2335.
[14] S. Felton, M. Tolley, E. Demaine, D. Rus, R. Wood, *Science* **2014**, *345*, 644.
[15] A. Lendlein, R. Langer, *Science* **2002**, *296*, 1673.
[16] H. He, J. Guan, J. L. Lee, *J. Controlled Release* **2006**, *110*, 339.
[17] L. Ionov, *Adv. Funct. Mater.* **2013**, *23*, 4555.
[18] S. K. Leist, J. Zhou, *Virtual Phys. Prototyping* **2016**, *11*, 249.
[19] T. Bückmann, N. Stenger, M. Kadic, J. Kaschke, A. Frölich, T. Kennerknecht, C. Eberl, M. Thiel, M. Wegener, *Adv. Mater.* **2012**, *24*, 2710.
[20] B. H. Cumpston, S. P. Ananthavel, S. Barlow, D. L. Dyer, J. E. Ehrlich, L. L. Erskine, A. A. Heikal, S. M. Kuebler, I.-Y. S. Lee, D. McCord-Maughon, J. Qin, H. Röckel, M. Rumi, X.-L. Wu, S. R. Marder, J. W. Perry, *Nature* **1999**, *398*, 51.
[21] K.-S. Lee, R. H. Kim, D.-Y. Yang, S. H. Park, *Prog. Polym. Sci.* **2008**, *33*, 631.
[22] D. Karalekas, A. Aggelopoulos, *J. Mater. Process. Technol.* **2003**, *136*, 146.
[23] M. P. Patel, M. Braden, K. W. M. Davy, *Biomaterials* **1987**, *8*, 53.
[24] H.-B. Sun, T. Suwa, K. Takada, R. P. Zaccaria, M.-S. Kim, K.-S. Lee, S. Kawata, *Appl. Phys. Lett.* **2004**, *85*, 3708.
[25] S. Maruo, T. Hasegawa, N. Yoshimura, *Opt. Express* **2009**, *17*, 20945.
[26] Q. Sun, K. Ueno, H. Misawa, *Opt. Lett.* **2012**, *37*, 710.
[27] A. V. Tobolsky, F. Leonard, G. P. Roeser, *J. Polym. Sci.* **1948**, *3*, 604.
[28] W. Xiong, Y. Liu, L. J. Jiang, Y. S. Zhou, D. W. Li, L. Jiang, J.-F. Silvain, Y. F. Lu, *Adv. Mater.* **2016**, *28*, 2002.
[29] E. D. Lemma, F. Rizzi, T. Dattoma, B. Spagnolo, L. Sileo, A. Qualtieri, M. De Vittorio, F. Pisanello, *IEEE Trans. Nanotechnol.* **2017**, *16*, 23.
[30] S. Timoshenko, *J. Opt. Soc. Am.* **1925**, *11*, 233.
[31] R. H. Saul, *J. Appl. Phys.* **1969**, *40*, 3273.
[32] C. Yoon, R. Xiao, J. Park, J. Cha, T. D. Nguyen, D. H. Gracias, *Smart Mater. Struct.* **2014**, *23*, 94008.
[33] F. Claeyssens, E. A. Hasan, A. Gaidukeviciute, D. S. Achilleos, A. Ranella, C. Reinhardt, A. Ovsianikov, X. Shizhou, C. Fotakis, M. Vamvakaki, B. N. Chichkov, M. Farsari, *Langmuir* **2009**, *25*, 3219.
[34] L. Wen, J. C. Weaver, G. V. Lauder, *J. Exp. Biol.* **2014**, *217*, 1656.
[35] A. Ovsianikov, X. Shizhou, M. Farsari, M. Vamvakaki, C. Fotakis, B. N. Chichkov, *Opt. Express* **2009**, *17*, 2143.
[36] W. C. Oliver, G. M. Pharr, *J. Mater. Res.* **1992**, *7*, 1564.